Kovove Mater. 60 2022 293–302
DOI: 10.31577/km.2022.5.293

Investigation of the effect of shot blasting on the surface properties of the HA coatings processed by the EPD method

Ali İhsan Bahçepinar*, İbrahim Aydin

Manisa Celal Bayar University, Vocational School of Technical Sciences, Machinery and Metal Technologies Department, Manisa, Turkey

Received 11 August 2021, received in revised form 19 July 2022, accepted 21 July 2022

Abstract

316L stainless steel implant material surfaces shot blasted with glass beads underwent hydroxyapatite (HA) coating process by electrophoretic deposition method (EPD). The mechanical and metallographic test results of HA coatings applied to the shot blasted and sanded substrates have been discussed. The sanded process was carried out with 320 Grit SiC sandpaper. Shot blasted process was carried out in a vacuum shot blasting machine at 5 bar pressure with glass beads. Ethanol was used as a solvent during the coating process. The coating solution was prepared by mixing ethanol, HA, PVA, and N, N-Dimethylformamide chemicals in specific ratios to have a steady suspension. Regarding tests conducted on HA coatings, it was revealed that shot blasted surfaces had better results when compared to those of sanded surfaces. Hopefully, this new process for coatings will be a new impression for future studies.

Key words: electrophoretic deposition, hydroxyapatite, shot blasting, coating

1. Introduction

Biomaterials are natural or synthetic materials used to replace organs or tissues that have lost their role in the human body. These materials are classified into four groups: metals, polymers, ceramics, and composites [1, 2].

Metallic biomaterials such as Ti and its alloys, Co--Cr alloys, and 316L stainless steels are used in most dental and orthopedic applications because of their high biocompatibility and mechanical properties. 316L stainless steels are commonly used for easy machinability, high mechanical properties, and low cost [3].

In the human body, ions such as protein, water, and chloride create a corrosive environment for metal implant materials [4]. Implants used in the body for a long time can be affected by this corrosive environment. This effect creates the possibility of the release of ions in the structure of the metal into the body. Ions such as Cr and Ni in the structure of the 316L implant have carcinogenic and allergenic effects [3]. Therefore, direct application of metal implants such as 316L is not widely accepted.

HA is one of the calcium phosphate-based materials with high biocompatibility and bioactivity, which is the main inorganic component of human bones and teeth [5–9]. HA is preferred in implantation applications because of its osteoconductive and biocompatibility properties [9–13]. However, due to its low mechanical properties, it cannot be directly used as an implant material [2, 9, 14–16].

Since the direct application of metallic biomaterials is not supported in implantation applications, it is preferable to use HA coatings with high biocompatibility and bioactivity [5, 17, 18]. With this application, a superior biomaterial is obtained by combining high bioactivity and biocompatibility with excellent mechanical properties. HA cuts the contact of metal ions with the body and prevents the release of ions into the body [2, 5, 19]. Also, the osteoconductive feature of HA enables implants to adhere tightly to the bone [20–22]. HA is the most widely used bioactive substance, supporting bone growth [2, 14, 23, 24].

There are several methods for the coating of metal implant material. These methods are as follows: plasma spray coating, spray coating, electrochemical deposition, electrophoretic deposition (EPD), dip coating, thermal spray coating, sol-gel, and

*Corresponding author: e-mail address: ali.bahcepinar@cbu.edu.tr

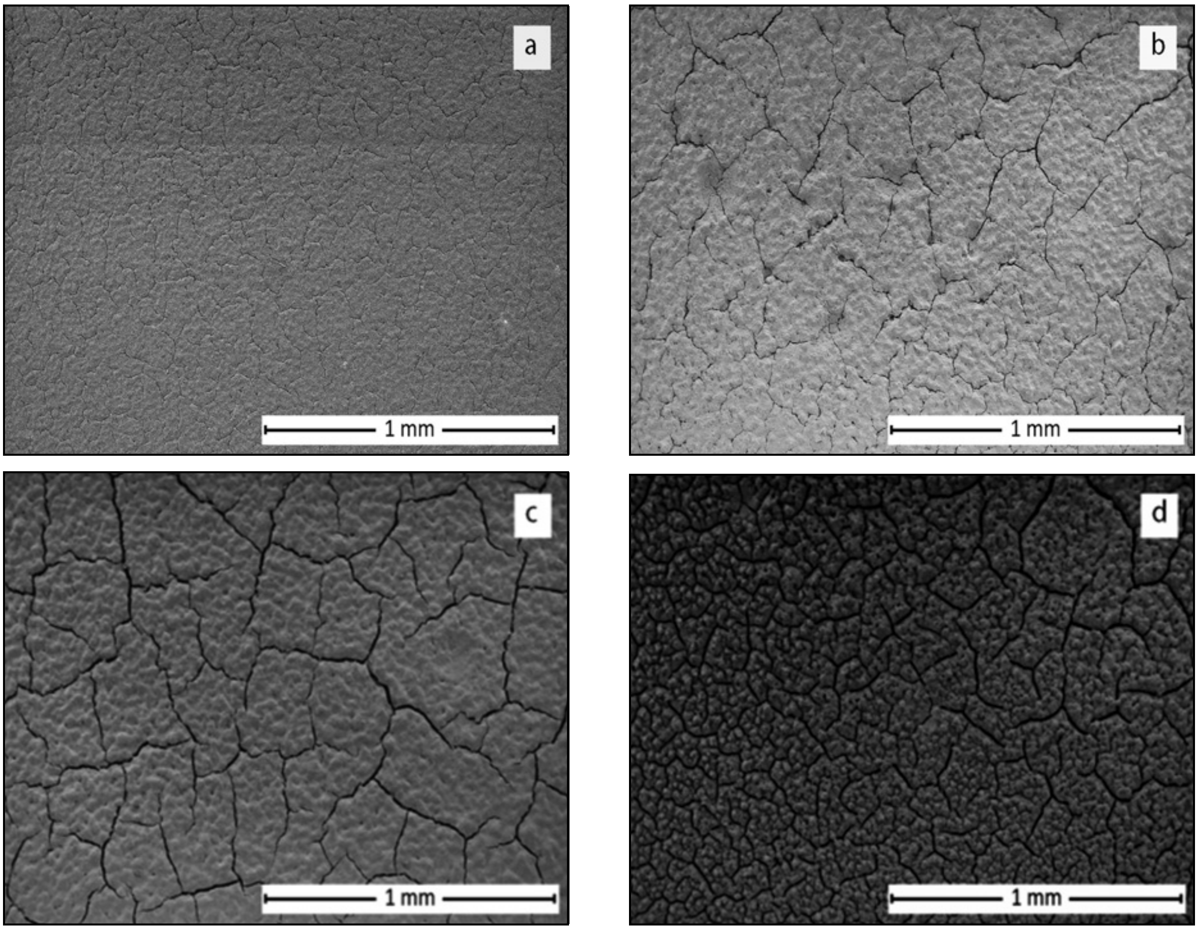

Fig. 1. 100× SEM images of the sanded substrate after coating: (a) 60 V/90 s, (b) 120 V/90 s, (c) 180 V/90 s, and (d) 240 V/90 s [40].

biomimetic method [1, 2, 25–32]. EPD has been an attractive method for hydroxyapatite coating processes in recent years [32, 33]. EPD is a method that begins with the movement of charged particles in a stable suspension under the influence of an electrical field to the opposite loaded metal implant material and is completed by the accumulation of charged particles on the implant material surface [32–35]. The main reasons why EPD is attractive are its characteristics such as the simple method, the low cost of the equipment, the ability to coat materials in complex geometries, to obtain homogeneous coatings, and to control the microstructure of the coating with a simple adjustment [32–37].

The surface preparation of the metal implant before the coating process is one of the important factors that determine the coating quality. To obtain a strong HA-implant coating, dirtiness on the metal implant surface must be cleaned, and appropriate surface roughness on the implant material surface must be provided [38].

This study aimed to examine the effect of shot blasting applied on the surface of the implant material before coating on the surface and the mechanical properties of the coating.

2. Materials and methods

2.1. Implant material selection and preparation of implants

316L stainless steel was used as a substrate. The 316L stainless steel substrate was cut in ø $20 \times 10\ \mathrm{mm}^2$. Some of the cut substrates were sanded with 320 SiC sandpaper. Some substrates were shot blasted with glass beads under 5 bar pressure in a vacuum shot blasting machine. The main purpose of shot blasting and sanding is to roughen the surface of the substrate and to clean the dirt on the surface. In the first stage, the substrate was cleaned in detergent water. Later, it was washed in an ultrasonic bath with distilled water for 30 min. After that, it was washed in an ultrasonic bath for 30 min in ethyl alcohol, rinsed with distilled water, and dried. To clean the oxide layers on the substrate surface, a solution was prepared by adding 2 ml of HF and 3 ml of HNO_3 to 100 ml of distilled water. In this solution, the substrates were kept for 2 min. At the last stage, they were kept in distilled water for 30 min in an ultrasonic bath. The cleaned substrates were dried in the oven and made ready for the coating process.

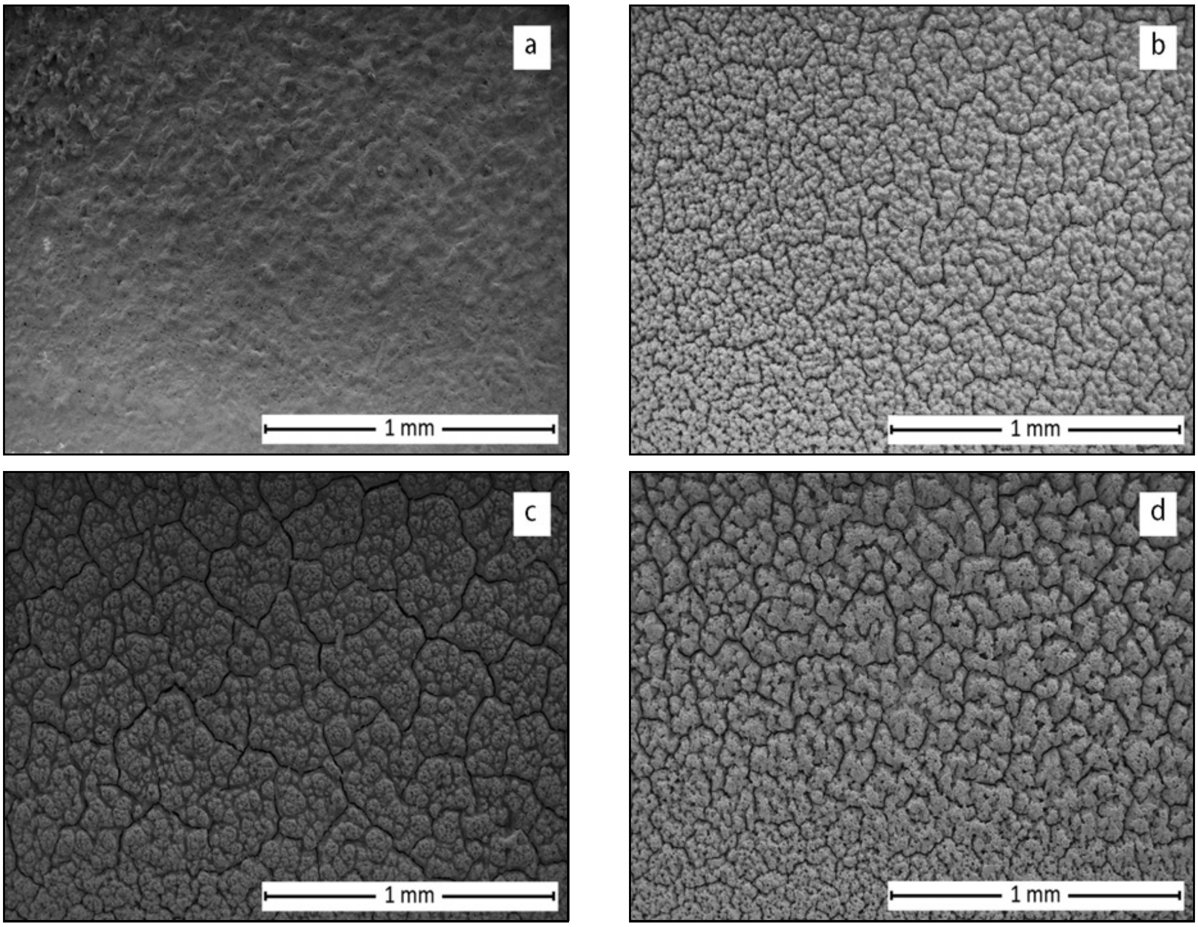

Fig. 2. 100× SEM images of shot blasted substrate after coating: (a) 60 V/90 s, (b) 120 V/90 s, (c) 180 V/90 s, and (d) 240 V/90 s [40].

2.2. The preparation of the coating

Ethanol of 99.8 percent purity was used as a solvent to prepare the coating suspension in the electrophoretic deposition process. 1 g of HA (NanoTech), 1 g of PVA (Merck, 72000), and 10 mL of N, N-Dimethylformamide (Sigma-Aldrich) were added to 100 mL of ethanol and mixed in a magnetic stirrer for 30 min to disperse the HA particles homogeneously. The mixing was done in a teflon beaker. To increase the adhesion strength of HA particles, PVA and N, N-Dimethylformamide was added to the suspension [39]. To ensure the stability of the prepared suspension, the pH was adjusted to 4 with the addition of HNO_3 and NaOH. The substrates used in the coating process were arranged so that their surfaces faced each other. The distance between the substrates was fixed at 10 mm. Prepared substrates were immersed in a stable suspension and connected to the DC power source (Bio RAD Powerpac Basic). The coating process was carried out in 90 s of deposition time and 60, 120, 180, and 240 V voltage values.

3. Results

3.1. SEM-EDX results

The microstructure analysis of the coated substrate was performed using the QUANTA 250 FEG model scanning electron microscope. Figures 1 and 2 show 100× scaled SEM images of coatings obtained at 60, 120, 180, and 240 V voltage values and 90 s accumulation time on sanded and shot blasted substrate. When Figs. 1 and 2 are examined, it is clear that HA coating covers the surface of the substrate in a homogeneous and intense manner. This shows that the coatings are successfully realized in all parameters. Furthermore, it is understood that the increased amount of applied voltage causes the coating to form a more cracked structure.

The elemental components of the coated substrate structures were determined using an EDX detector on the QUANTA 250 FEG model scanning electron microscope. The EDS results for different coating parameters are given in Figs. 3 and 4. According to the EDS analysis results, the weight percentages and Ca/P ratios of the atomic structures of the calcium and phos-

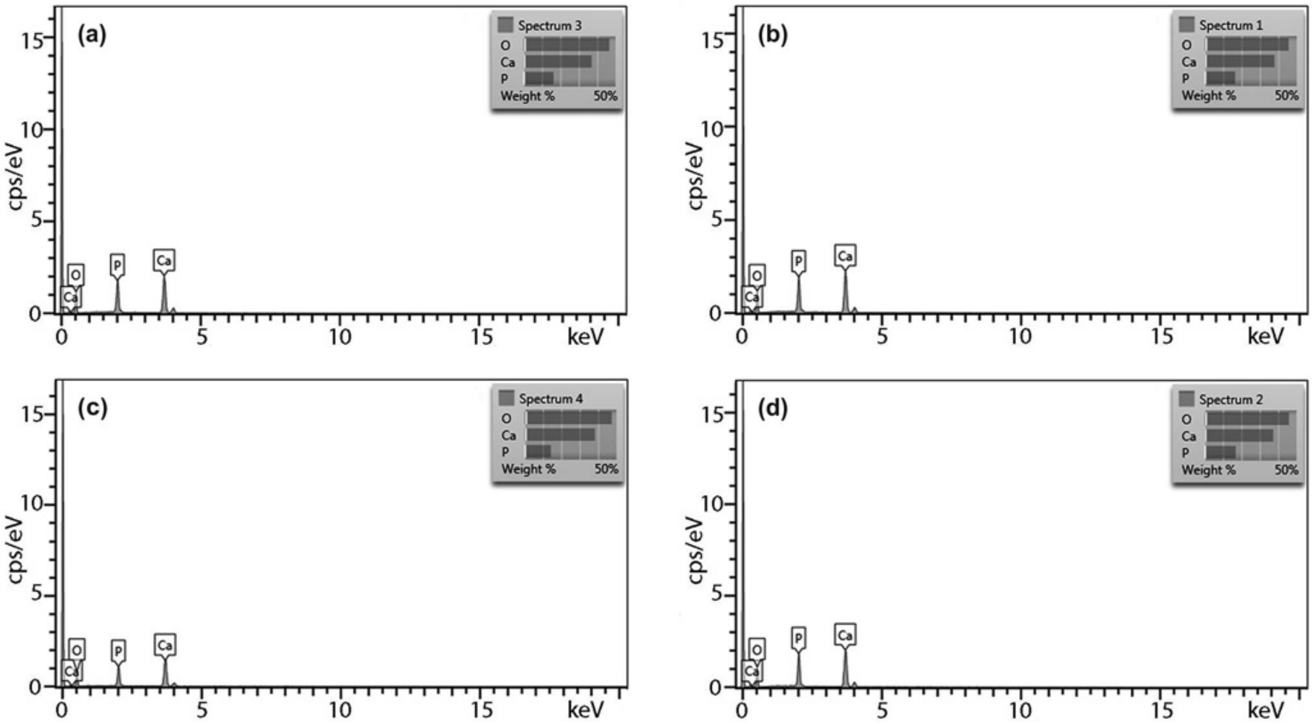

Fig. 3. EDS analysis results of coating surfaces formed on sanded substrate: (a) 60 V/90 s, (b) 120 V/90 s, (c) 180 V/90 s, and (d) 240 V/90 s [40].

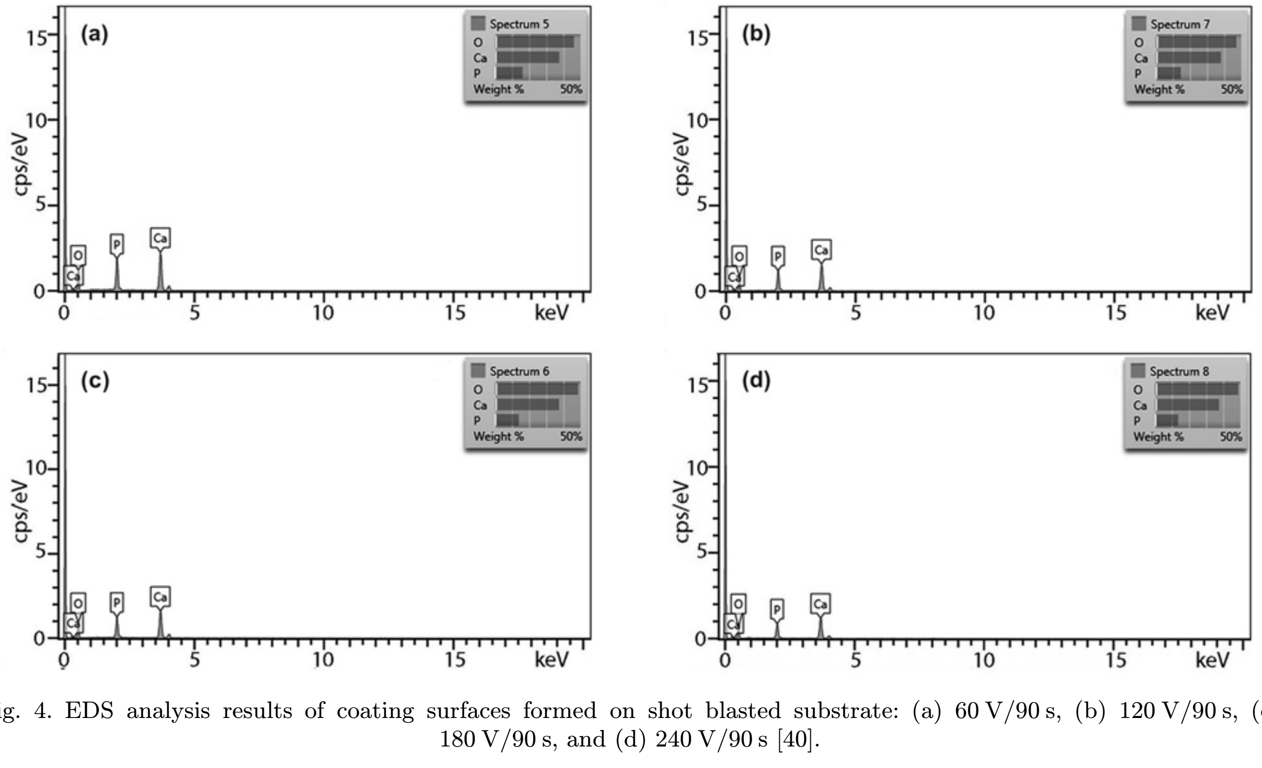

Fig. 4. EDS analysis results of coating surfaces formed on shot blasted substrate: (a) 60 V/90 s, (b) 120 V/90 s, (c) 180 V/90 s, and (d) 240 V/90 s [40].

phate elements formed on the surfaces of the substrate of all parameters are given in Table 1. When the results of the EDS analysis are examined, it can be seen that the calcium phosphate structure is obtained in all the coatings parameters.

3.2. XRD results

To determine which phases the coated substrate contained and the concentrations of these phases, a PHILIPS X'PERT PRO X-radiation diffraction device

Table 1. Atomic weight ratios and Ca/P ratios of calcium and phosphate elements forming on coating surfaces for all coating parameters [40]

Coating parameters	% Ca ratio	% P ratio	Ca/P ratio
Sanded substrate – 60 V/90 s	21.44	12.54	1.71
Sanded substrate – 120 V/90 s	21.17	12.07	1.75
Sanded substrate – 180 V/90 s	21.82	12.33	1.77
Sanded substrate – 240 V/90 s	21.80	10.54	2.06
Shot blasted substrate – 60 V/90 s	21.84	12.01	1.82
Shot blasted substrate – 120 V/90 s	21.75	10.86	2.00
Shot blasted substrate – 180 V/90 s	21.14	10.21	2.07
Shot blasted substrate – 240 V/90 s	21.13	9.98	2.11

Table 2. Coating thickness results for all parameters [40]

Coating parameters	Coating thickness (μm)
Sanded substrate – 60V/90 s	3.83 ± 0.146
Sanded substrate –120V/90 s	4.91 ± 0.184
Sanded substrate – 180V/90 s	5.23 ± 0.339
Shot blasted substrate – 240V/90 s	6.86 ± 0.473
Shot blasted substrate – 60V/90 s	3.88 ± 0.158
Shot blasted substrate – 120V/90 s	5.01 ± 0.226
Shot blasted substrate – 180V/90 s	5.85 ± 0.273
Shot blasted substrate – 240V/90 s	7.12 ± 0.554

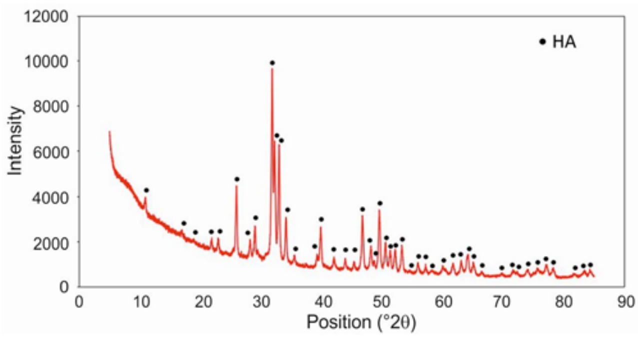

Fig. 5. XRD result [40].

was used. Figure 5 shows the results derived from the XRD analysis. The XRD analysis was performed by scraping HA powder off the substrate surface. According to the test results, the apatite crystals occurred at peak points of 25.97°, 29.03°, 31.14°, 31.28°, 31.86°, 33.00°, 39.88°, 46.74°, 49.52°, and 53.24°.

3.3. Coating thickness results

The thickness of the HA coatings was evaluated in terms of μm using an ElektroPhysik MiniTest 730/Sensor FN 1.5 HD trademark device. The averages of the results were taken by performing evaluations on each coating surface five times. The average values of the coating thicknesses gained from the evaluation results are given in Table 2. When examining Table 2, it is seen that the coated thickness values of the shot blasted substrate are higher than those of the sanded substrate. In addition, it is seen that the coated thickness increases with the increase in the amount of applied voltage.

3.4. Surface roughness results

For the determination of the surface roughness values of the substrate gained by the result of the coatings, Roughness Tester (PCE-RT 1200) device was used. The averages of the results were taken by performing evaluations on each coating surface five times. The average roughness values gained by the evaluation results are given in Table 3.

3.5. Vickers indentation test results

The microhardness and elasticity modulus of HA coating were determined with the help of nanoindentation tests. In the indentation process carried out under a 5 mN load, the Berkovich tip type was used. At least 3 measurements were made for each substrate, and microhardness and elasticity modulus values were calculated by taking the average of these measurement results. The test results are shown in Table 4.

3.6. Scratch test results

Scratch test equipment was used in the Middle East University Technical Research & Development

Table 3. Surface roughness results for all parameters [40]

Coating parameters	Surface roughness (μm)
Sanded substrate – 60 V/90 s	0.971 ± 0.111
Sanded substrate – 120 V/90 s	1.396 ± 0.128
Sanded substrate – 180 V/90 s	1.715 ± 0.150
Sanded substrate – 240 V/90 s	2.113 ± 0.187
Shot blasted substrate – 60 V/90 s	1.127 ± 0.115
Shot blasted substrate – 120 V/90 s	1.412 ± 0.139
Shot blasted substrate – 180 V/90 s	1.801 ± 0.160
Shot blasted substrate – 240 V/90 s	2.385 ± 0.173

Table 4. Vickers hardness and elasticity modulus values for all coating parameters [40]

Coating parameters	Vickers hardness (MPa)	Elasticity modulus (GPa)
Sanded substrate – 60 V/90 s	231.134	34.166
Sanded substrate – 120 V/90 s	206.219	29.837
Sanded substrate – 180 V/90 s	120.207	18.148
Sanded substrate – 240 V/90 s	68.510	7.551
Shot blasted substrate – 60 V/90 s	208.429	29.926
Shot blasted substrate – 120 V/90 s	158.056	16.691
Shot blasted substrate – 180 V/90 s	110.873	14.897
Shot blasted substrate – 240 V/90 s	34.620	6.455

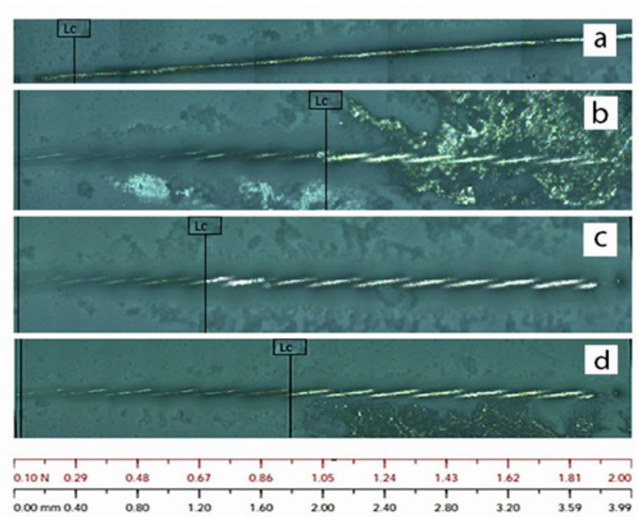

Fig. 6. Optical microscope images of the scratch test results of coatings on sanded substrate: (a) 60 V/90 s, (b) 120 V/90 s, (c) 180 V/90 s, and (d) 240 V/90 s [40].

Training and Measurement Center to measure the bonding strength of the layering on the surface. The load range was set at 0.1–2 N, scratch length was 4 mm, and scratch speed was 1.5 mm min^{-1}. Under these conditions, all experiments were performed. Figures 6 and 7 show optical microscope scratch pictures derived from the experiment. Table 5 shows the critical load values after loading applied up to 2 N to the surface of the sanded substrate. When Fig. 7 is exam-

Table 5. Critical load values for all parameters of coatings on a sanded substrate [40]

Coating parameters	Critical load (N)
Sanded substrate – 60 V/90 s	0.65
Sanded substrate – 120 V/90 s	1.03
Sanded substrate – 180 V/90 s	0.69
Sanded substrate – 240 V/90 s	0.955

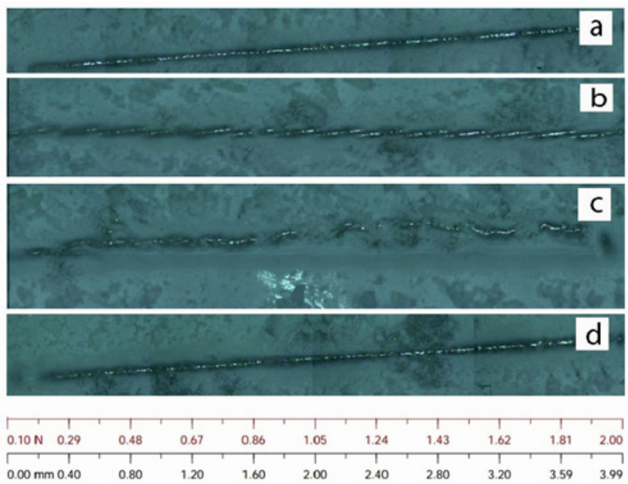

Fig. 7. Optical microscope images of the scratch test results of coatings on shot blasted substrate: (a) 60 V/90 s, (b) 120 V/90 s, (c) 180 V/90 s, and (d) 240 V/90 s [40].

ined, it is seen that the substrate cannot be entirely reached after the applied loading up to 2 N. The critical load value is, therefore, > 2.

4. Discussion

Drevet et al. [34] observed the Ca/P ratio of 1.66 in the HA coatings made on Ti6Al4V implants by the EPD method at 10V voltage and 10 min of deposition time. Aydin et al. [2] observed the Ca/P ratios of 1.61, 1.65, 1.72, and 1.73 in the HA coatings made on Ti6Al7Nb implants by the EPD method. Aydin et al. [41] observed the Ca/P ratios as 1.59, 1.63, 1.66, and 1.72 in the HA coatings obtained by the EPD method with different parameters on AZ91 magnesium alloy implants. The ideal Ca/P ratio was determined in the literature for HA covers at 1.67 [42]. Table 1 provides the results of the Ca/P values calculated in the study. Values close to the ideal Ca/P ratio are seen in all parameters.

Aydin et al. [2] observed HA crystals at peak points of $2\theta = 26.0078°$, 28.1945°, 32.2494°, 34.1778°, 39.9130°, 48.1571°, and 50.5511° in the XRD result of the HA coatings which they had created on the surface of T6Al7Nb alloy by EPD method. Kumar et al. [23] observed HA crystals at peak points of $2\theta = 26.06°$, 31.62° in XRD result of the HA coatings created on the surface of Mg-3Zn alloy by the EPD method. Iqbal et al. [8] observed HA crystals at peak points of 25.91°, 28.94°, 31.78°, 32.19°, 32.93°, 34.10°, 39.80°, 46.71°, and 49.49° in XRD result of the HA coatings which they created on the surface of 316L stainless steel by EPD method. Aydin et al. [41] observed HA crystals at peak points of $2\theta = 25.7182°$, 28.7945°, 31.6402°, 32.0520°, 32.6648°, 32.7802°, 33.8369°, 33.926°, 39.6934°, 46.2985°, 49.3822°, and 70.7743° in XRD result of the HA coatings which they created on the surface of AZ91 magnesium alloy by EPD method. In this study, HA crystals were observed at peaks of 25.97°, 29.03°, 31.14°, 31.28°, 31.86°, 33.00°, 39.88°, 46.74°, 49.52°, and 53.24°. This showed that HA powders preserved their structure during electrophoretic deposition, as in the literature.

Aydin et al. [2] determined the coating thickness as 4.38, 5.43, 7.60, and 9.42 μm, respectively, on the HA coatings, which they performed on Ti6Al7Nb alloy. Aydin et al. [41] determined the coating thickness as 5.86, 7.73, 9.72, and 12.11 μm on the HA coatings, which they performed on AZ91 magnesium alloy. Kwok et al. [19] determined the coating thickness as approximately 10 μm in the HA coatings, which they performed on Ti6Al4V alloy. Bartmanski et al. [43] determined the coating thickness as approximately 29.35 μm in the HA coatings, which they performed on Ti13Zr13Nb alloy. Dudek et al. [28] determined the coating thickness as 2.6, 2.8, and 4.2 μm in the HA coatings, which they performed on NiTi shape memory alloy.

The increased voltage in the EPD process caused coarser particles to accumulate. Increasing the number of coarse particles on the substrate surface increased the surface roughness value [5]. Wennenberg [44] determined the optimal surface roughness as 1–1.5 μm in its study of implant materials with varying surface roughness. When examining the results of surface ruggedness values specified in Table 3, successful results are seen. After the shot blasting process, the surface roughness value of the substrate material was measured as 2.66 μm, and the surface roughness value of the substrate material after the sanding process was 0.34 μm. Increasing the surface roughness of the implants will increase the placement of HA particles in the apertures formed on the implant surface; it can provide a strong attachment between the implant and HA particles [45].

Aydin et al. [2] observed the surface roughness values as 0.818, 1.055, 1.552, and 1.673 μm on the HA coatings, which they performed on Ti6Al7Nb alloy. Aydin et al. [41] observed the surface roughness values as 1.18, 1.95, 2.26, and 2.83 μm on the HA coatings, which they performed on AZ91 magnesium alloy. Bartmanski et al. [43] observed the surface roughness values as 1.26 μm on the HA coatings, which they performed on Ti13Zr13Nb alloy. Javidi et al. [5] observed the surface roughness values as 1.8 μm on the HA coatings, which they performed on 316L stainless steel alloy.

The elasticity modulus and hardness values of metal materials used in implantation processes are high. However, these values are low in human bone. In the HA coatings performed in this study, properties similar to the mechanical properties of the bone were obtained. There are differences in the mechanical properties of the bones in different parts of the human body. For example, the modulus of elasticity is 0.001–0.01 GPa in joint cartilage, 0.05–0.5 GPa in cancellous bone, 1 GPa in tendon bone, and 7–30 GPa in shell bone [4]. It has been observed that the mechanical properties obtained in all covering parameters are applicable to shell bone implants. In addition, coatings with poor mechanical properties can be quickly dissolved in the human body. Therefore, mechanical properties are an important parameter for the applicability of implants. The fact that the mechanical properties of the coatings are similar to the bone eliminates the stiffness incompatibility between the bone and the implant.

Drevet et al. [34] observed that the hardness value was 5.4–153.5 MPa and the elasticity modulus value was 5.2–19 GPa in HA coatings which they performed on Ti6Al4V alloy. Bartmanski et al. [43] observed that the hardness value was 0.0112–0.1349 GPa and the elasticity modulus value was between 1.25–30.31 GPa in HA coatings which they performed on Ti13Zr13Nb.

On the optical microscope images obtained as a result of the scratch tests of HA coatings in Figs. 6 and 7, it is seen that the adhesion strength of the HA coatings applied to the substrate shot blasted is higher than that of the HA coatings applied to the sanded substrate. This shows the effectiveness of the shot blasting process before coating on the adhesion of the coating. Bartmanski et al. [43] determined the critical load values as 29.15–92.48 mN on the HA coatings, which they performed on Ti6Al7Nb alloy. Drevet et al. [34] determined the critical load value as 3.3 N on the HA coating, which they performed on Ti6Al7Nb alloy. Kumar et al. [23] determined the critical load values as 0.691–1.32 N on the HA coatings, which they performed on Mg-3Zn alloy.

5. Conclusions

In this study, HA coating process by the EPD method was performed on 316L stainless steel implants whose surface was sanded and shot blasted. The mechanical and metallographic results obtained after the study were evaluated.

When the SEM images of the HA coatings created as a result of the study are examined, it is seen that there are homogeneous coatings that intensely surround the implant material in all parameters. Also, it has been observed as the applied voltage increases, the cracks on the surface increase.

When the EDS analysis results are examined, it is observed that the calcium phosphate structure was formed in all parameters. The ideal Ca/P ratio of HA coatings in the literature has been determined as 1.67 [42]. When the Ca/P values calculated in the study are examined, it is seen that there are values close to the ideal Ca/P ratio in all parameters.

When the results for surface roughness are examined, the surface roughness of coating is shown to increase with the increase in the voltage value. The surface roughness values of the sanded substrate applied coatings were between 0.971–2.113 μm, and the surface roughness values of the coatings on shot blasted substrates were obtained between 1.127–2.385 μm. The surface roughness values of HA coating on shotblasted substrates are higher. The ideal surface roughness was measured between 1–1.5 μm [44]. Coatings with ideal surface roughness value are obtained in 90 s accumulation time at 60 and 120 V voltage applied to shot blasted and sanded substrate.

When the coating thickness results are examined, it is seen that the coating thickness increases as the voltage value increases. The coating thickness of the sanded substrate applied coatings was between 3.83–6.86 μm, and the coating thickness of the shot blasted substrate applied coatings was between 3.88–7.12 μm. When the results are examined, the coating thickness of HA coating applied to the shot blasted substrate is seen to be of higher value.

When the indentation test results are examined, the hardness and elasticity modulus for the coatings decrease when the voltage value increases. The hardness values of the HA coatings on sanded substrates are between 231.134–68.510 MPa and the elastic modulus values are between 34.166–7.551 GPa. The hardness values of the HA coatings on shot blasted substrates are between 208.429—34.620 MPa and the elastic modulus values are between 29.926–6.455 GPa. Elasticity modulus value is 0.001–0.01 GPa in joint cartilage, 0.05–0.5 GPa in cancellous bone, 1 GPa in tendon bone, and 7–30 GPa in shell bone [4]. It has been observed that HA coatings obtained in all parameters can become applicable to shell bone implants.

When the optical microscope images obtained from the scratch tests of HA coatings applied on the shot blasted and sanded substrates are compared, it has been determined that the adhesion strength of the HA coatings applied to the shot blasted substrate is higher than that of the HA coatings applied to the sanded substrate. This demonstrated the effectiveness of the shot blasting process before coating on the adhesion of the coating.

References

[1] I. Aydin, F. Engin, Hydroxyapatite coating on Ti6Al4V alloy surface through biomimetic method using glycolic acid – Sodium gluconate buffer system and examination of properties of the coating, Journal of Polytechnic 20 (2017) 993–1001. https://doi.org/10.2339/politeknik.369141

[2] I. Aydin, A. I. Bahcepinar, M. Kirman, M. A. Cipiloğlu, HA coating on Ti6Al7Nb alloy using an electrophoretic deposition method and surface properties examination of the resulting coatings, Coatings 9 (2019) 402. https://doi.org/10.3390/coatings9060402

[3] K. Prabakaran, T. V. Thamaraiselvi, S. Rajeswari, Electrochemical evaluation of hydroxyapatite reinforced phosphoric acid treated 316L stainless steel, Trends Biomaterials 19 (2016) 84–87.

[4] I. Aydin, H. Cetinel, A. Pasinli, M. Yuksel, Preparation of hydroxyapatite coating by using citric acid sodium citrate buffer system in the biomimetic procedure, Materials Testing 55 (2013) 782–788. https://doi.org/10.3139/120.110501

[5] M. Javidi, S. Javadpour, M. E. Bahrololoom, J. Ma, Electrophoretic deposition of natural hydroxyapatite on medical grade 316L stainless steel, Mat. Sci. Eng. C 28 (2008) 1509–1515. https://doi.org/10.1016/j.msec.2008.04.003

[6] I. Bogdanoviciene, A. Beganskiene, K. Tõnsuaadu, J. Glaser, H.-J. Meyer, A. Kareiva, Calcium hydroxyapatite, $Ca_{10}(PO_4)_6(OH)_2$ ceramics prepared by aqueous sol-gel processing, Mater. Res. Bull. 41 (2006)

1754–1762.
https://doi.org/10.1016/j.materresbull.2006.02.016

[7] F. R. Morteza, Electrophoretic deposition of hydroxyapatite nanoparticles: Effect of suspension composition on the electrochemical potential difference at deposit/suspensions interface, Mater. Res. Express 5 (2018) 085005.
https://doi.org/10.1088/2053-1591/aad1a2

[8] N. Iqbal, R. Nazir, A. Asif, A. A. Chaudhry, M. Akram, G. Y. Fan, A. Akram, R. Amin, S. H. Park, R. Hussain, Electrophoretic deposition of PVA coated hydroxyapatite on 316L stainless steel, Curr. Appl. Phys. 12 (2012) 755–759.
https://doi.org/10.1016/j.cap.2011.11.003

[9] Q. Tian, J. Lin, L. Rivera-Castaneda, A. Tsanhani, Z. S. Dunn, A. Rodriguez, A. Aslani, H. Liu, Nano-to-submicron hydroxyapatite coatings for magnesium-based bioresorbable implants – Deposition, characterization, degradation, mechanical properties, and cytocompatibility, Scientific Reports 9 (2019) 810.
https://doi.org/10.1038/s41598-018-37123-3

[10] M. Chambard, O. Marsan, C. Charvillat, D. Grossin, P. Fort, C. Rey, F. Gitzhofer, G. Bertrand, Effect of the deposition route on the microstructure of plasma-sprayed hydroxyapatite coatings, Surface and Coatings Technology 371 (2019) 68–77.
https://doi.org/10.1016/j.surfcoat.2019.01.027

[11] R. B. Heimann, Plasma-sprayed hydroxylapatite-based coatings: Chemical, mechanical, microstructural, and biomedical properties, Journal of Thermal Spray Technology 25 (2016) 827–850.
https://doi.org/10.1007/s11666-016-0421-9

[12] R. A. Surmenev, A review of plasma-assisted methods for calcium phosphate based coatings fabrication, Surface and Coatings Technology 206 (2012) 2035–2056.
https://doi.org/10.1016/j.surfcoat.2011.11.002

[13] K. Suchanek, A. Bartkowiak, M. Perzanowski, M. Marszałek, M. Sowa, W. Simka, Electrochemical properties and bioactivity of hydroxyapatite coatings prepared by MEA/EDTA double-regulated hydrothermal synthesis, Electrochimica Acta 298 (2019) 685–693.
https://doi.org/10.1016/j.electacta.2018.12.140

[14] G. Miranda, F. Sousa, M. M. Costa, F. Bartolomeu, F. S. Silva, O. Carvalho, Surface design using laser technology for Ti6Al4V-hydroxyapatite implants, Opt. Laser Technol. 109 (2019) 488–495.
https://doi.org/10.1016/j.optlastec.2018.08.034

[15] J. Luo, X. Jia, R. Gu, P. Zhou, Y. Huang, J. Sun, M. Yan, 316L stainless steel manufactured by selective laser melting and its biocompatibility with or without hydroxyapatite coating, Metals 8 (2018) 548.
https://doi.org/10.3390/met8070548

[16] H. Zhou, J. Lee, Nanoscale hydroxyapatite particles for bone tissue engineering, Acta Biomaterialia 7 (2011) 2769–2781.
https://doi.org/10.1016/j.actbio.2011.03.019

[17] M. Curcio, J. V. Rau, A. Santagata, R. Teghil, S. Laureti, A. De Bonis, Laser synthesis of iron nanoparticle for Fe doped hydroxyapatite coatings, Materials Chemistry and Physics 225 (2019) 365–370.
https://doi.org/10.1016/j.matchemphys.2018.12.099

[18] W. Zhou, Z. Hu, T. Wang, G. Yang, W. Xi, Y. Gan, W. Lu, J. Hu, Enhanced corrosion resistance and bioactivity of Mg alloy modified by Zn-doped nanowhisker hydroxyapatite coatings, Colloids and Surfaces B: Biointerfaces 186 (2020) 110710.
https://doi.org/10.1016/j.colsurfb.2019.110710

[19] C. T. Kwok, P. K. Wong, F. T. Cheng, H. C. Man, Characterization and corrosion behavior of hydroxyapatite coatings on Ti6Al4V fabricated by electrophoretic deposition, Appl. Surf. Sci. 255 (2009) 6736–6744.
https://doi.org/10.1016/j.apsusc.2009.02.086

[20] P. Wongwitwichot, J. Kaewsrichan, K. H. Chua, B. H. I. Ruszymah, Comparison of TCP and TCP/HA hybrid scaffolds for osteoconductive activity, The Open Biomedical Engineering Journal 4 (2010) 279–285.
https://doi.org/10.2174/1874120701004010279

[21] Y. Yeom, B. Hwang, D. Yang, H. I. Shin, S. Hahn, Effect of osteoconductive hyaluronate hydrogels on calvarial bone regeneration, Biomaterials Research 18 (2014) 8. https://doi.org/10.1186/2055-7124-18-8

[22] M. N. Rahaman, W. Xiao, Y. Liu, B. Sonny Bal, Osteoconductive and Osteoinductive Implants Composed of Hollow Hydroxyapatite Microspheres, In: Advances in Bioceramics and Porous Ceramics VII (2015) 65–79. https://doi.org/10.1002/9781119040392.ch7

[23] R. M. Kumar, K. K. Kuntal, S. Singh, P. Gupta, B. Bhushan, P. Gopinath, D. Lahiri, Electrophoretic deposition of hydroxyapatite coating on Mg-3Zn alloy for orthopaedic application, Surf. Coat. Tech. 287 (2016) 82–92.
https://doi.org/10.1016/j.surfcoat.2015.12.086

[24] D. A. Wahl, J. T. Czernuszka, Collagen-hydroxyapatite composites for hard tissue repair, European Cells and Materials 11 (2006) 43–56.
https://doi.org/10.22203/eCM.v011a06

[25] L. F. Rodrigues Jr., M. C. Tronco, C. F. Escobar, A. S. Rocha, L. A. L. Santos, Painting method for hydroxyapatite coating on titanium substrate, Ceramics International 45 (2019) 14806–14815.
https://doi.org/10.1016/j.ceramint.2019.04.211

[26] R. I. M. Asri, W. S. W. Harun, M. A. Hassan, S. A. C. Ghani, Z. Buyong, A review of hydroxyapatite-based coating techniques: Sol-gel and electrochemical depositions on biocompatible metals, Journal of the Mechanical Behavior of Biomedical Materials 57 (2016) 95–108. https://doi.org/10.1016/j.jmbbm.2015.11.031

[27] J. Qi, Z. Chen, W. Han, D. He, Y. Yang, Q. Wang, Effect of deposition parameters and heat treatment on the microstructure, mechanical and electrochemical properties of hydroxyapatite/titanium coating deposited on Ti6Al4V by RF-magnetron sputtering, Materials Research Express 4 (2017) 096409.
https://doi.org/10.1088/2053-1591/aa8a7e

[28] K. Dudek, T. Goryczka, Electrophoretic deposition and characterization of thin hydroxyapatite coatings formed on the surface of NiTi shape memory alloy, Ceram. Int. 42 (2016) 19124–19132.
https://doi.org/10.1016/j.ceramint.2016.09.074

[29] H.-N. Yu, H.-C. Hsu, S.-C. Wu, C.-W. Hsu, S.-K. Hsu, W.-F. Ho, Characterization of nano-scale hydroxyapatite coating synthesized from eggshells through hydrothermal reaction on commercially pure titanium, Coatings 10 (2020) 112.
https://doi.org/10.3390/coatings10020112

[30] A. M. Vilardell, N. Cinca, N. Garcia-Giralt, S. Dosta, I. G. Cano, X. Nogués, J. M. Guilemany, In-vitro comparison of hydroxyapatite coatings obtained by cold spray and conventional thermal spray technologies, Materials Science and Engineering: C 107 (2020) 110306. https://doi.org/10.1016/j.msec.2019.110306

[31] T. A. Ngo, S. Hiromoto, S. T. Pham, N. Q. Cao, Adhesion properties of hydroxyapatite and octacalcium phosphate coating layers to AZ31 alloy formed at various pH values, Surface and Coatings Technology 381 (2020) 125187. https://doi.org/10.1016/j.surfcoat.2019.125187

[32] A. Pawlik, M. A. U. Rehman, Q. Nawaz, F. E. Bastan, G. D. Sulka, A. R. Boccaccini, Fabrication and characterization of electrophoretically deposited chitosan-hydroxyapatite composite coatings on anodic titanium dioxide layers, Electrochimica Acta 307 (2019) 465–473. https://doi.org/10.1016/j.electacta.2019.03.195

[33] E. Avcu, F. E. Baştan, H. Z. Abdullah, M. A. U. Rehman, Y. Y. Avcu, A. R. Boccaccini, Electrophoretic deposition of chitosan-based composite coatings for biomedical applications: A review, Progress in Materials Science 103 (2019) 69–108. https://doi.org/10.1016/j.pmatsci.2019.01.001 .

[34] R. Drevet, N. Ben Jaber, J. Fauré, A. Tara, A. Ben Cheikh, H. Benhayoune, Electrophoretic deposition (EPD) of nano-hydroxyapatite coatings with improved mechanical properties on prosthetic Ti6Al4V substrates, Surf. Coat. Tech. 301 (2016) 94–99. https://doi.org/10.1016/j.surfcoat.2015.12.058

[35] A. Molaei, M. Lashgaroo, M. Yousefpour, Effects of electrophoretic parameters on chitosan-based nanocomposite coatings, Journal of the Australian Ceramic Society 56 (2020) 1–10. https://doi.org/10.1007/s41779-019-00413-8

[36] S. Singh, G. Singh, N. Bala, Corrosion behavior and characterization of HA/Fe_3O_4/CS composite coatings on AZ91 Mg alloy by electrophoretic deposition, Materials Chemistry and Physics 237 (2019) 121884. https://doi.org/10.1016/j.matchemphys.2019.121884

[37] N. Horandghadim, J. Khalil-Allafi, M. Urgen, Influence of tantalum pentoxide secondary phase on surface features and mechanical properties of hydroxyapatite coating on NiTi alloy produced by electrophoretic deposition, Surface and Coatings Technology 386 (2020) 125458. https://doi.org/10.1016/j.surfcoat.2020.125458

[38] M. Jażdżewska, B. Majkowska-Marzec, Hydroxyapatite deposition on the laser modified Ti13Nb13Zr alloy, Advances in Materials Science 17 (2017) 5–13. https://doi.org/10.1515/adms-2017-0017

[39] A. R. Boccaccini, S. Keim, R. Ma, Y. Li, I. Zhitomirsky, Review: Electrophoretic deposition of biomaterials, Journal of The Royal Society Interface 7 (2010) S581–S613. https://doi.org/10.1098/rsif.2010.0156.focus

[40] A. I. Bahcepinar, Investigation of the effect of sandblasting on the surface properties of the HA coatings processed with EPD method, [Master Thesis], Manisa Celal Bayar University Institute of Science and Technology, Manisa, Turkey (2020).

[41] I. Aydin, A. I. Bahçepinar, C. Gūl, Surface characterization of EPD coating on AZ91 Mg alloy produced by powder metallurgy, Revista de Metalurgia 56 (2020) 176. https://doi.org/10.3989/revmetalm.176 .

[42] M. R. Urist, A. Lietze, E. Dawson, β tricalcium delivery system for bone morphogenetic protein, Clinical Orthopedics and Related Research 187 (1984) 227-280.

[43] M. Bartmanski, A. Zielinski, B. Majkowska-Marzec, G. Strugala, Effects of solution composition and electrophoretic deposition voltage on various properties of nanohydroxyapatite coatings on the Ti13Zr13Nb alloy, Ceramics International 44 (2018) 19236–19246. https://doi.org/10.1016/j.ceramint.2018.07.148 .

[44] A. Wennerberg, The importance of surface roughness for implant incorporation, International Journal of Machine Tools and Manufacture 38 (1998) 657–662. https://doi.org/10.1016/s0890-6955(97)00114-4 .

[45] S. A. X. Stango, D. Karthick, S. Swaroop, U. K. Mudali, U. Vijayalakshmi, Development of hydroxyapatite coatings on laser textured 316 LSS and Ti-6Al-4V and its electrochemical behavior in SBF solution for orthopedic applications, Ceramics International 44 (2018) 3149–3160. https://doi.org/10.1016/j.ceramint.2017.11.083